Advanced Concepts for Hydrogen Storage

John J. Petrovic
Materials Science and Technology Division
Los Alamos National Laboratory

DOE Hydrogen Storage Workshop
Argonne National Laboratory
14-15 August 2002

Advanced Concepts Topics

- The following topics were identified by me through an in-depth review of the recent technical literature to search out new materials areas that might, with more research, have potential for improved hydrogen storage:
  - Advanced hydride materials
  - Hydride “alcoholysis”
  - BN nanotubes
  - Zeolites
  - Mesoporous materials
  - Nanosize metal powders
  - Hydrogen from iron hydrolysis
- These and other contributed ideas will be discussed by the Advanced Concepts Working Group

Advanced Hydride Materials

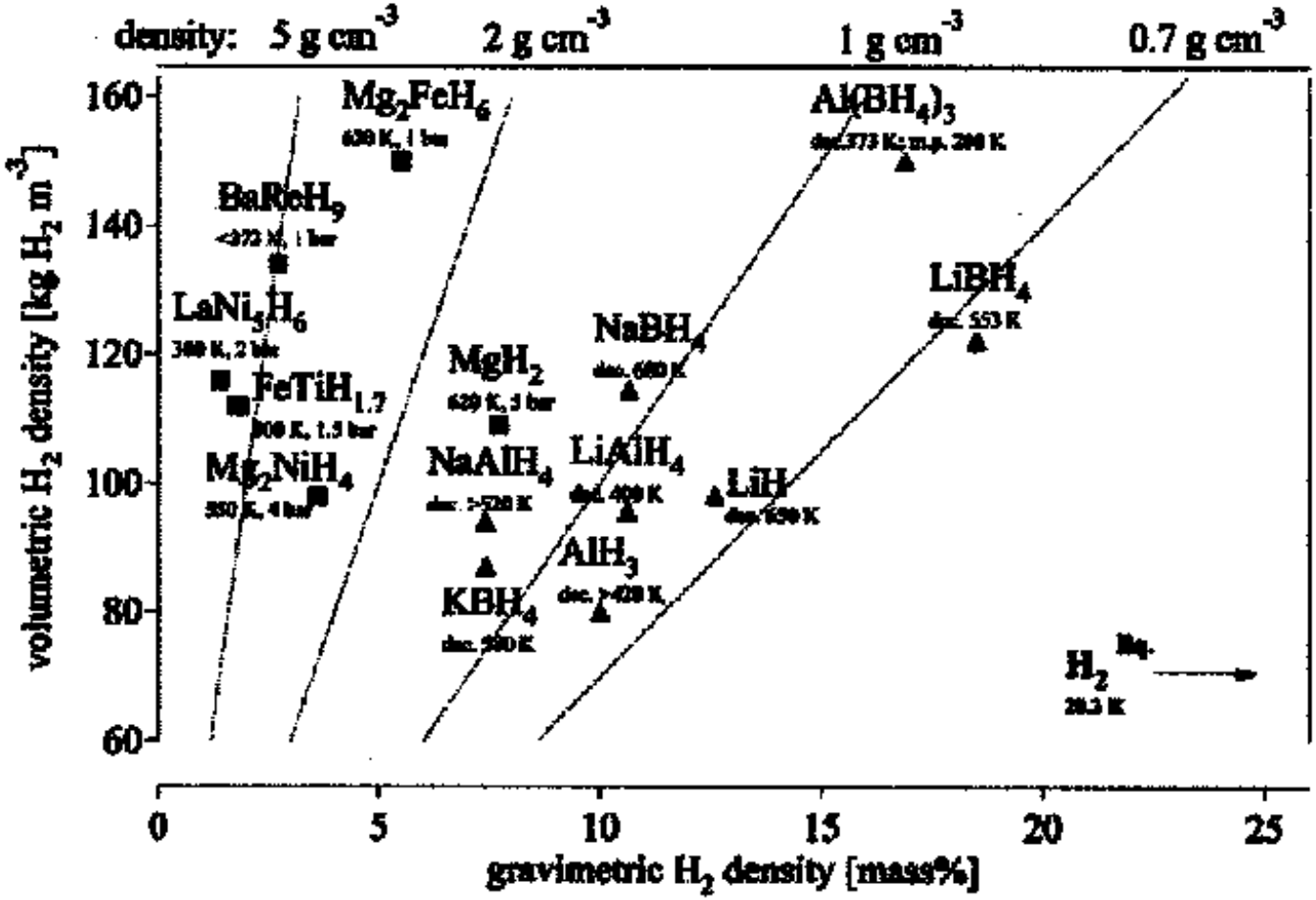

A. Zuttel, et.al., “Hydrogen Desorption From Lithiumtetrahydroboride ($LiBH_4$), Proceedings, 14th World Hydrogen Energy Conference, June 2002, Montreal, Canada.

Hydrogen Generation from $LiBH_4$

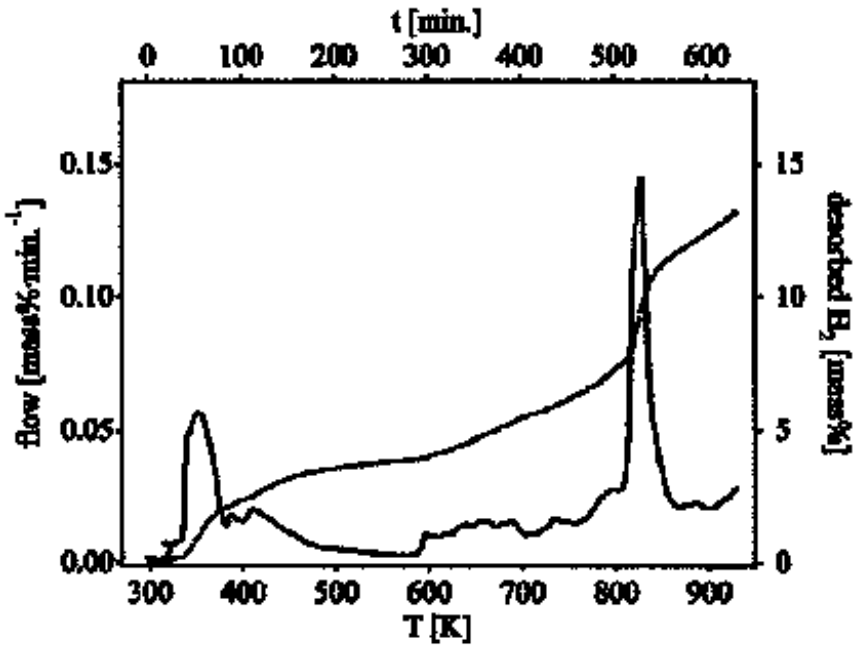

- $LiBH_4$ (lithium tetrahydroboride)
  - Salt-like, hydroscopic, crystalline material
  - Density 0.68 g/cm^3
  - Melting point 275°C
- $LiBH_4 = LiH + B + 1.5H_2(g)$
  - DG becomes negative at 450°C
  - Endothermic reaction
  - 13.8 wt.% H_2 released
- A low temperature H_2 release has been observed
  - 2.3 wt.% H_2 released at 118°C
  - May be related to an orthorhmbic-to-tetragonal crystallographic change
    - **Is this a reversible process?**

A. Zuttel, et.al., "Hydrogen Desorption From Lithiumtetrahydroboride ($LiBH_4$), Proceedings, 14th World Hydrogen Energy Conference, June 2002, Montreal, Canada.

Hydrolysis of $LiBH_4$-Organics

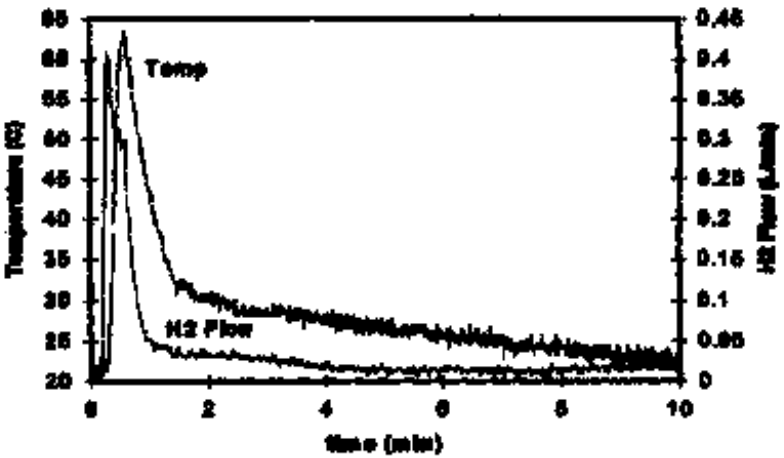

Fig. 3. Data acquired in the hydrolysis of compound 2.

Organics combined with $LiBH_4$ to reduce the severity and heat of the hydrolysis reaction

$$\{M(L)BH_4\}_x + 4xH_2O \rightarrow 4xH_2 + xMOH + xB(OH)_3 + xL$$

M = lithium

L = organic ligand

- **Compound 1:**
  - $[HC(3,5\text{-}Me_2pz)_3]LiBH_4$
- Molecular weight of organics in the range of 300 g/mol

Table 3. Hydrogen yields and maximum temperatures

Compound	$NaBH_4$	1	2	3	4	5	6
Hydrogen Yield[a] (% of theoretical)	89, 96	88, 100	98	56, 68	84	76, 87	104, 101
Maximum Temp (°C)	87, 98	52, 67	63	84, 54	60	45, 45	55, 36

(1) $[HC(3,5\text{-}Me_2pz)_3]LiBH_4$; (2) $\{[H_2C(3,5\text{-}Me_2pz)_2]Li(BH_4)\}_2$; (3) $[(TMEDA)Li(BH_4)]_2$; (4) $[HC(pz)_3]LiBH_4$; (5) $\{[H_2C(pz)_2]Li(BH_4)\}_2$; (6) $Mg(BH_4)_2 \cdot 3THF$.
[a] accuracy is estimated to be ±5%.

Table 2. Heats of hydrolysis reaction of the novel hydrides

Compound	$NaBH_4$	$LiBH_4$	1	2	4	5	6
kJ mol hydride	−267	−301	−255	−284	−216	−435	−414
kJ mol H_2 produced	−67	−75	−64	−36	−54	−54	−52
kJ kg reactants	−2431	−3211	−650	−477	−699	−898	−1000
kJ l reactants	−2496	−2879	−692	−509	−753	−995	−1200

(1) $[HC(3,5\text{-}Me_2pz)_3]LiBH_4$; (2) $\{[H_2C(3,5\text{-}Me_2pz)_2]Li(BH_4)\}_2$; (3) $[(TMEDA)Li(BH_4)]_2$; (4) $[HC(pz)_3]LiBH_4$; (5) $\{[H_2C(pz)_2]Li(BH_4)\}_2$; (6) $Mg(BH_4)_2 \cdot 3THF$.

2.5 wt.% H_2 produced from Compound 1

R. Aiello, M.A. Matthews, D.L. Reger, and J.E. Collins, "Production of Hydrogen Gas From Novel Chemical Hydrides", Int. J. Hydrogen Energy, 23, 1103-1108 (1998).

Chemical Reactions of Hydrides With Alcohols (Alcoholysis)

Hydride	wt. % of H_2 (in respect to the hydride weight)	Litres of H_2 obtained per 1 kg of hydride	Total H_2 capacity (including the weight of the hydride **and** the alcohol - methanol)
LiH	25.4	2845	5.0
$LiAlH_4$	13.2	1478	7.2
Li_3AlH_6	16.8	1882	6.1
$LiBH_4$	23.1	2592	9.4
NaH	8.3	933	3.6
$NaAlH_4$	9.3	1045	5.9
Na_3AlH_6	8.9	996	4.6
$NaBH_4$	13.3	1490	7.3
$Li_3Be_2H_7$	22.0	2460	7.1
Li_2BeH_4	22.5	2516	6.7
MgH_2	15.3	1716	4.5
CaH_2	9.6	1074	3.8
$FeTiH_2$	5.7	641	2.6
ZrH_2	4.3	484	2.6
TiH_2	8.1	905	3.5
$MgAl_2H_8$	11.7	1307	6.7
$LiAl_2H_7$	11.9	1329	8.1
$ZrAl_2H_8$	6.6	737	4.6

$$MH_x + x\,ROH \Rightarrow M(OR)_x + x\,H_2\uparrow$$

$$LiH + CH_3OH \rightarrow LiOCH_3 + H_2$$

$$NaH + CH_3OH \rightarrow NaOCH_3 + H_2$$

$$LiH + C_2H_5OH \rightarrow LiOC_2H_5 + H_2$$

$$MgH_2 + 2\,C_2H_5OH \rightarrow Mg(OC_2H_5)_2 + 2\,H_2$$

Controlled and convenient production of H_2 at room temperature and below room temperature

John Strom-Olsen, “Method of Hydrogen Generation for Fuel Cell Applications and a Hydrogen-Generating System”, Patent Filing WO0185606, May 2001, McGill University.

Hydrogen Adsorption by Boron Nitride Nanotubes

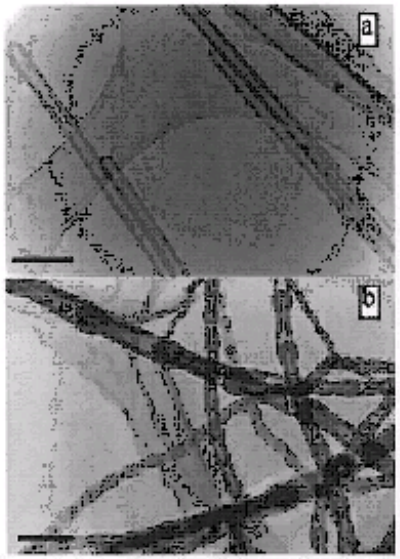

Figure 1 The morphologies of BN nanotubes: (a) multiwall nanotubes and (b) bamboo-like nanotubes. Scale bar: 100 nm.

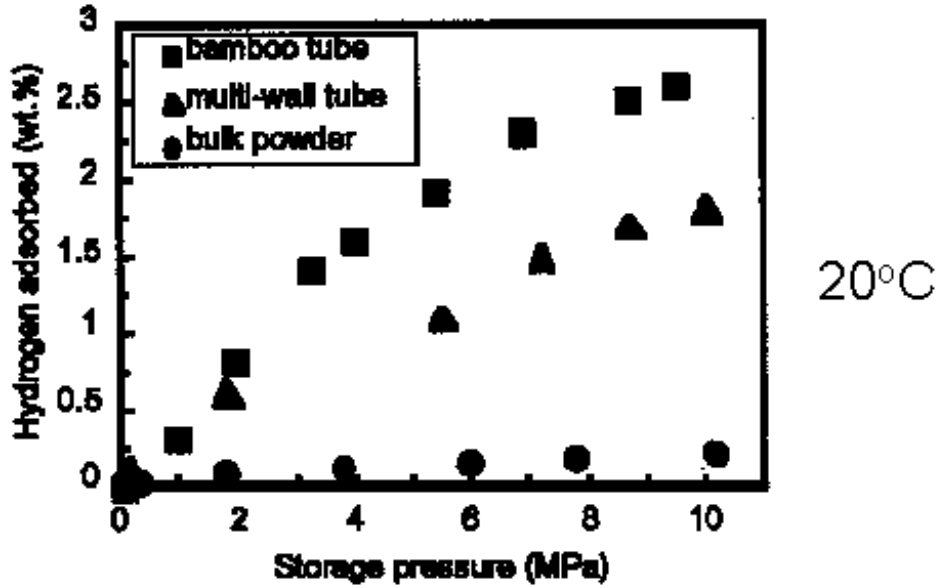

Figure 2 The hydrogen adsorption as a function of pressure in multiwall BN nanotubes and bamboo nanotubes at ~10 MPa is 1.8 and 2.6 wt %, respectively, in sharp contrast to the 0.2 wt % in bulk BN powder. The values reported here have an error of <0.3 wt %.

BN nanotubes synthesized through a chemical vapor deposition process by pyrolyzing a B-N-O precursor at 1730°C in a N_2/NH_3 atmosphere

R. Ma, Y. Bando, H.Zhu, T. Sato, C. Xu, and D. Wu, “Hydrogen Uptake in Boron Nitride Nanotubes at Room Temperature”, J. Am. Chem. Soc., 124, 7672-7673 (2002).

Zeolite Structures

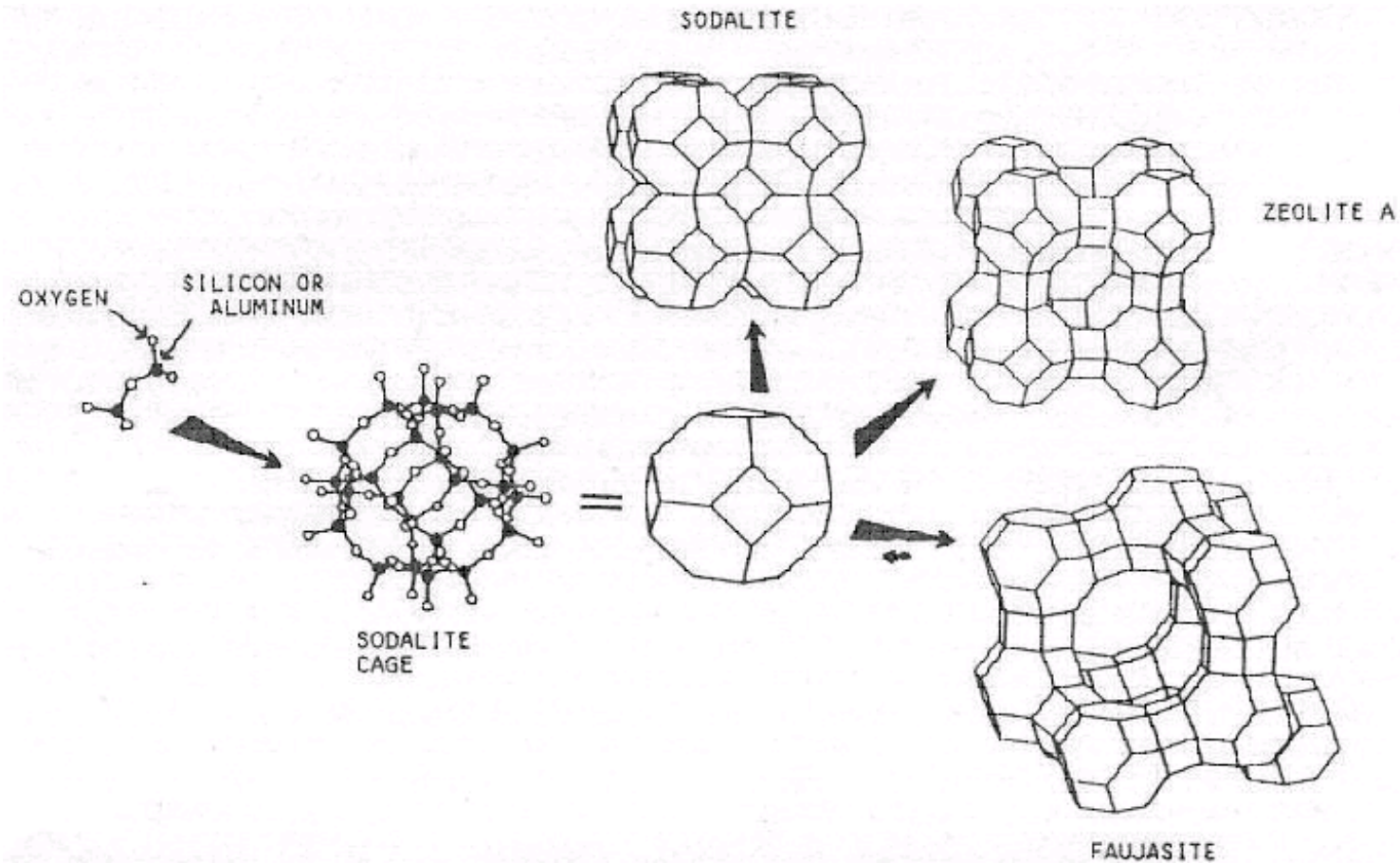

"Zeolite" is the Greek word for "boiling stone"

M.E. Davis, "Zeolites and Molecular Sieves: Not Just Ordinary Catalysts", Ind. Eng. Chem. Res., 30, 1675-1683 (1991).

Comparison of Carbon and Zeolite Hydrogen Physisorption

- Physisorption at 77°K and 1 bar pressure
- Activated carbon Norit 990293
  - BET surface area 2030 m^2/gm
  - 2.1 wt.% hydrogen adsorbed
    - Highest level of all carbon materials that were examined
- Zeolite ZSM-5
  - BET surface area 430 m^2/gm
  - 0.7 wt.% hydrogen adsorbed
    - Highest level of all silica-based materials that were examined

M.G. Nijkamp, J.E. Raaymakers, A.J. van Dillen, and K.P. de Jong, "Hydrogen Storage Using Physisorption – Materials Demands", Appl. Phys. A, 72, 619-623 (2001).

Modeling of Hydrogen Storage in Zeolite A

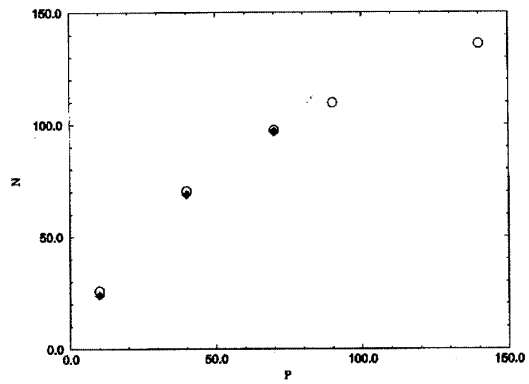

FIG. 3. Average numbers N_s and N_{exp} of H_2 molecules per unit cell of the zeolite computed by GCMC simulation (dot) (cf. Sec. III B) and measured experimentally (diamond) at $T=293$ K ($k_BT/\epsilon^{H_2H_2}=T^*=7.988$) with pressures ranging from 10 to 140 MPa.

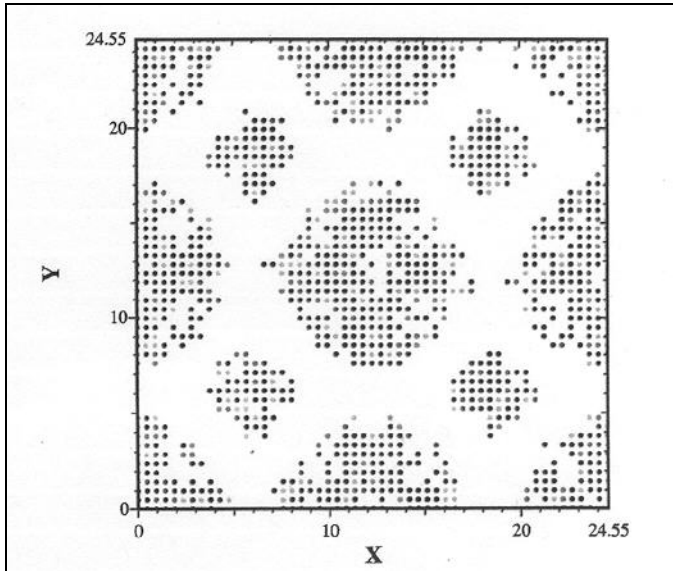

FIG. 4. Two-dimensional projection of the average local density of H_2 molecules in a unit cell of the NaA zeolite computed (cf. Sec. III B), at 10 MPa and $T^*=7.988$, from a GCMC simulation made of 2×10^6 MC steps. The dots show the domains where the average local density is different from zero. The shading of each dot indicates the value of the local density in a small subvolume of ~10 Å^3 around the dot position. The gray colors of the dots from white to black (black color is associated with the maximal local density) correspond to increasing values of the local density.

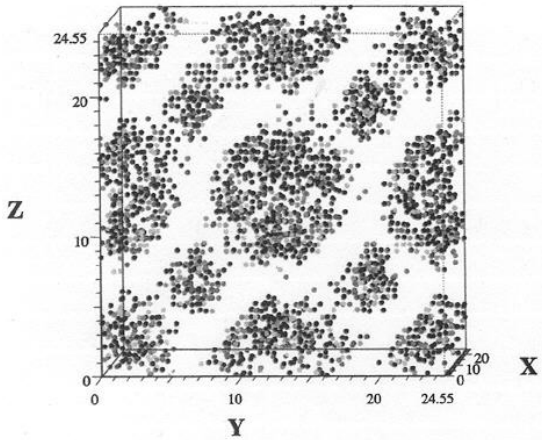

FIG. 5. Three-dimensional view of the average local density plotted in Fig. 4.

Modeling suggests that Zeolite A can store at least 2 wt.% H_2 if all cage sites are filled

F. Darkrim, A. Aoufi, P. Malbrunot, and D. Levesque, “Hydrogen Adsorption in the NaA Zeolite: A Comparison Between Numerical Simulations and Experiments”, Journal of Chemical Physics, 112, 5991-5999 (2000).

Large Pore Zeolite UTD-1

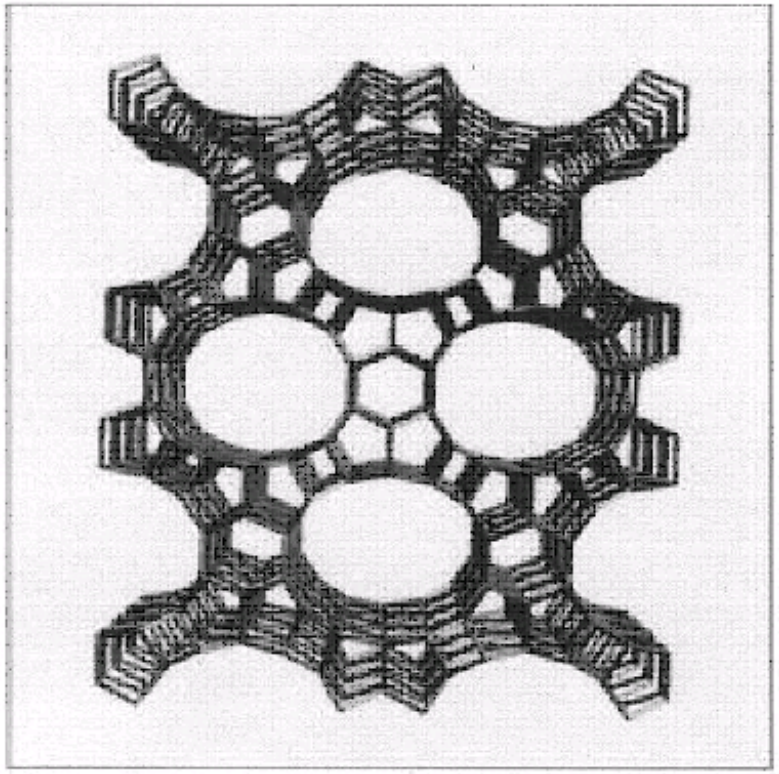

Figure 1. Framework structure of UTD-1 (oxygen atoms omitted for clarity) calculated with use of the crystallographic data in ref 38.

- High silica zeolite
  - SiO_2/Al_2O_3 ratio ~ 70
- 14-ring channel
- One-dimensional channel along [001]
- Channel dimensions of 1.0 x 0.75 nm

Hydrogen storage in large pore zeolites has never been examined

R.F. Lobo, et.al., "Characterization of the Extra-Large-Pore Zeolite UTD-1", J. Am. Chem. Soc., 119, 8474-8484 (1997).

Synthesis of Ordered Carbon Molecular Sieves by Templating

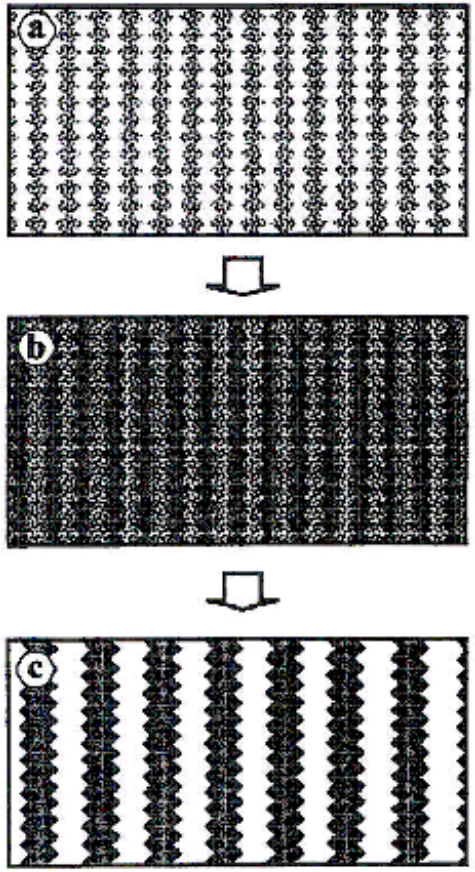

Figure 3. Schematic outline of the template synthesis procedure with silica molecular sieve: (a) The mesoporous silica molecular sieve MCM-48, (b) MCM-48 after completing carbonization within pores, and (c) CMK-1 obtained by removing the silica wall after carbonization.

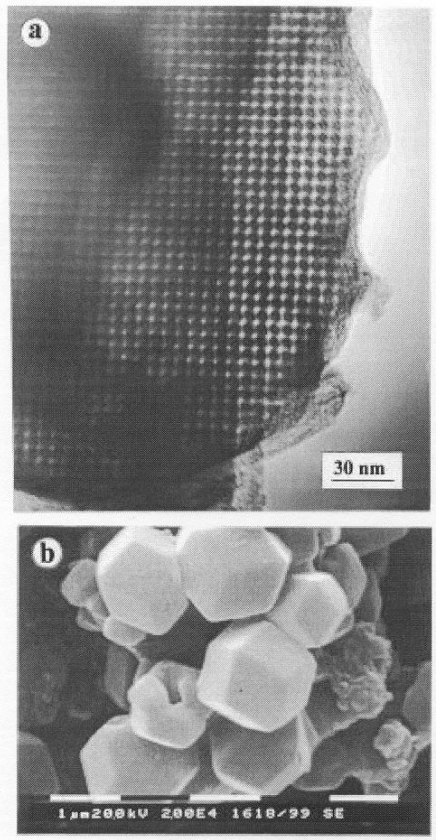

Figure 1. (a) Representative transmission electron micrograph of the ordered carbon molecular sieve CMK-1, obtained by the template synthesis with the mesoporous silica molecular sieve MCM-48. This image was obtained with a Philips CM20 transmission electron microscope operated at 100 kV from thin edges of a particle supported on porous carbon grid. (b) Scanning electron micrograph of a CMK-1 sample. This image was obtained on a Philips SEM-535M microscope using an acceleration voltage of 20.0 kV.

- Mesoporous silica molecular sieve MCM-48 impregnated with sucrose
- Sucrose converted to carbon by heating to 800-1100°C in vacuum or inert atmosphere
- Silica framework dissolved in aqueous solution of NaOH and ethanol

What are the hydrogen storage capabilities of this ordered carbon molecular sieve material?

R. Ryoo, S.H. Joo, and S. Jun, “Synthesis of Highly Ordered Carbon Molecular Sieves via Template-Mediated Structural Transformation”, J. Phys. Chem. B, 103, 7743-7746 (1999).

SiO_2 Xerogels and Aerogels

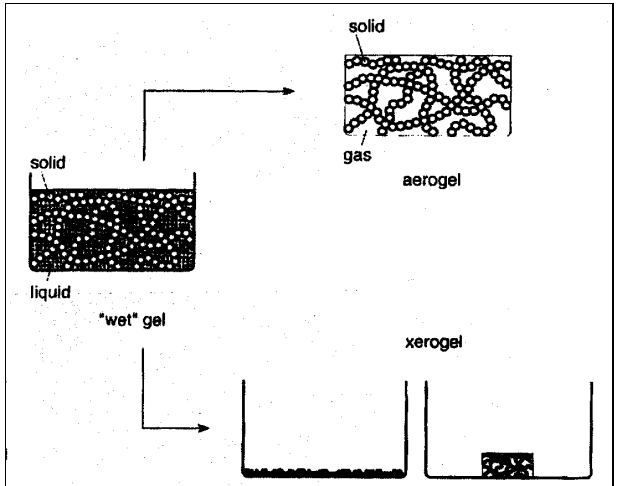

Figure 3. Shrinkage upon drying of a wet gel body to give an aerogel (top) and a xerogel (bottom) as a powder (left) and a monolith (right).

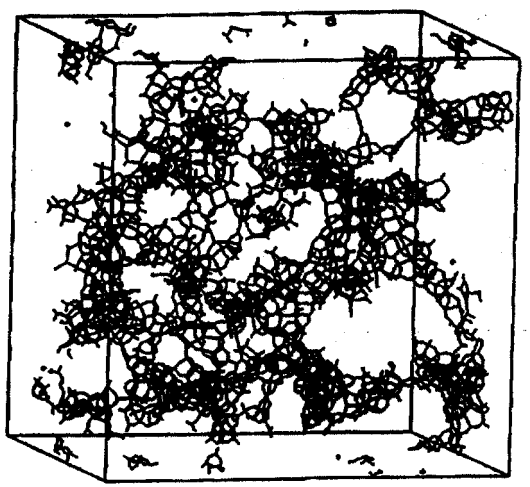

Figure 2. Schematic description of the structure of a silica aerogel (reproduced with friendly permission from ref. [6]).

- **Xerogels**
  - Produced by conventional drying of wet silica gel
- **Aerogels**
  - Produced by liquid-to-gas drying of wet silica gel
    - Supercritical fluid drying

Structural Properties of SiO_2 Aerogels

- Bulk density: 0.003-0.500 g/cm^3
- Porosity: 80% - 99.8%
- Mean pore diameter: 20-150 nm
- BET surface area: 100-1600 m^2/gm

No studies of hydrogen storage in SiO_2 xerogels and aerogels in the literature

N. Husing and U. Schubert, "Aerogels-Airy Materials: Chemistry, Structure, and Properties", Angew. Chem. Int. Ed., 37, 22-45 (1998).

Mesoporous Metal-Organic MOF-5

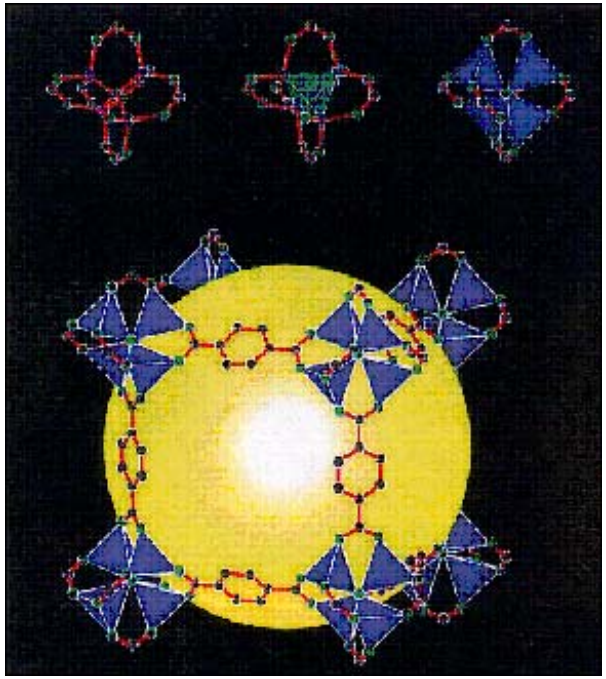

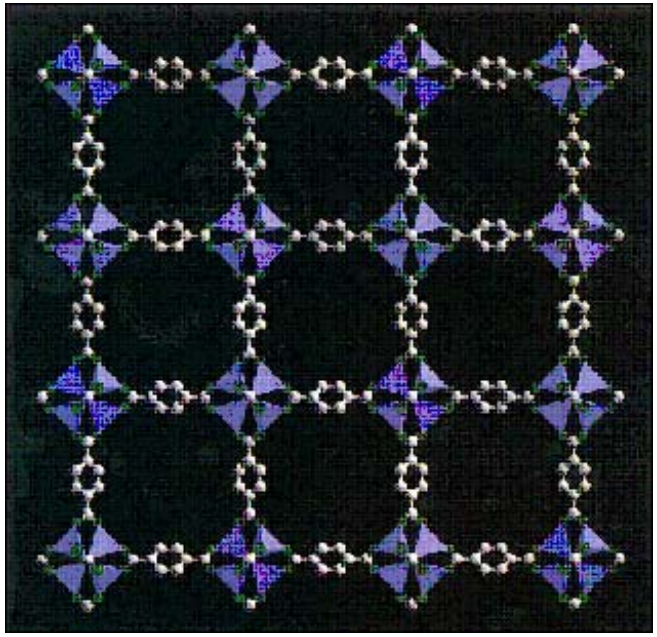

- Chemical formula $Zn_4O\ (BDC)_3\ (DMF)_8\ (C_6H_5Cl)$
  - BCD = 1,4 - benzenedicarboxylate
  - DMF = dimethylformamide
- ZnO_4 tetrahedral clusters linked together by C_6H_4-C-O_2 “struts”
- Cubic crystal structure
- 1.294 nm spacing between centers of adjacent clusters
- **What are the hydrogen storage characteristics of this material?**

H. Li, M. Eddaoudi, M. O’Keeffe, O.M. Yaghi, “Design and Synthesis of an Exceptionally Stable and Highly Porous Metal-Organic Framework”, Nature, 402, 276-279 (1999).

Mesoporous Organosilica Material

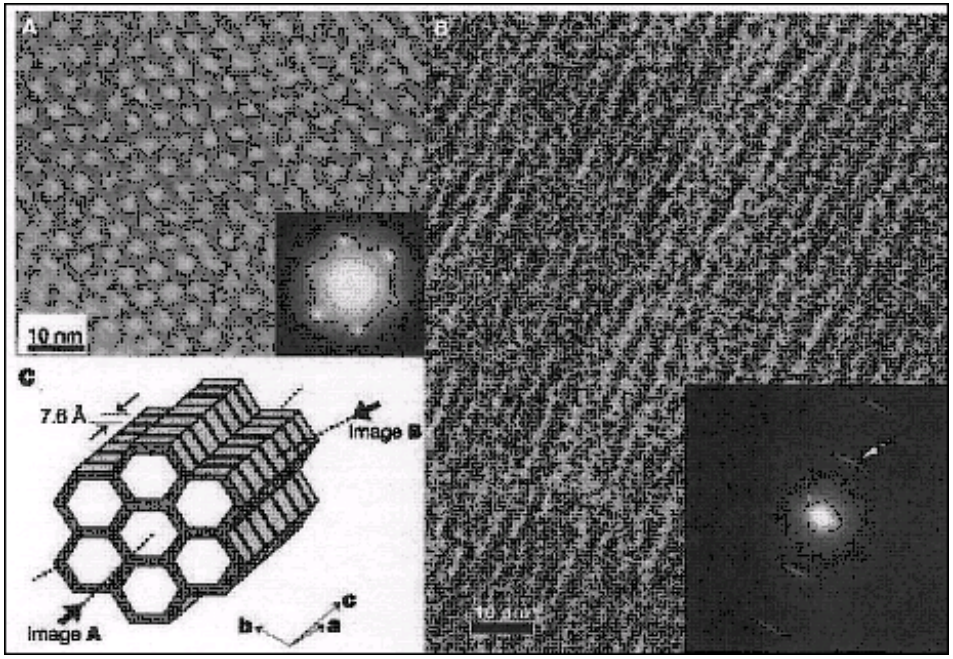

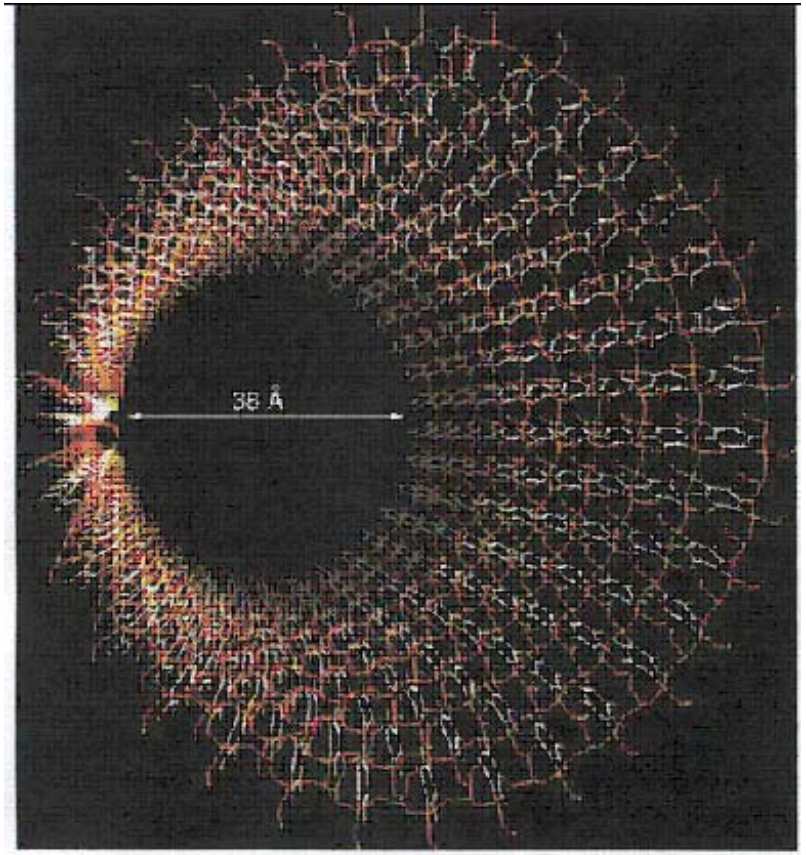

Figure 4 Model showing the pore surface of mesoporous benzene–silica. Benzene rings are aligned in a circle around the pore, fixed at both sides by silicate chains. The silicate is terminated by silanol (Si–OH) at the surface. Hydrophobic benzene layers and hydrophilic silicate layers array alternately at an interval of 7.6 Å along the channel direction. Silicon, orange; oxygen, red; carbon, white; hydrogen, yellow.

benzene-silica hybrid material

Hydrogen storage behavior?

S. Inagaki, S. Guan, T. Ohsuna, and O. Terasaki, “An Ordered Mesoporous Organosilica Hybrid Material With a Crystal-Like Wall Structure”, Nature, 416, 304-307 (2002).

Nanosize Metal and Ceramic Powders

- Nanosize metal and ceramic powders are commercially available
  - 10 - 100 nm diameters
- Nanosize metal powders
  - Au, Ag, Ni, Ti, Mo, Pt, W
- Nanosize ceramic powders
  - Al_2O_3, ZrO_2, CeO_2, CuO, MgO SiO_2, TiO_2

Gold-Thiol Single Molecule Electrical Junctions

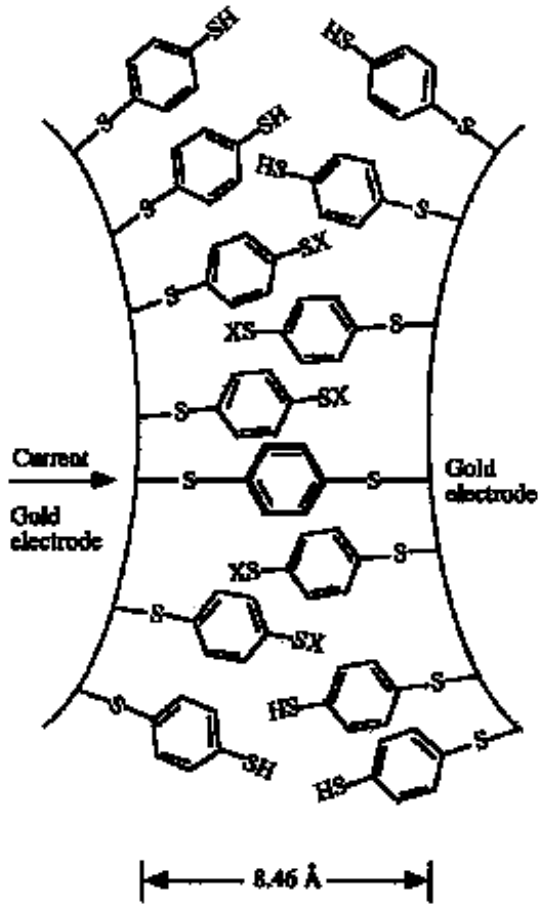

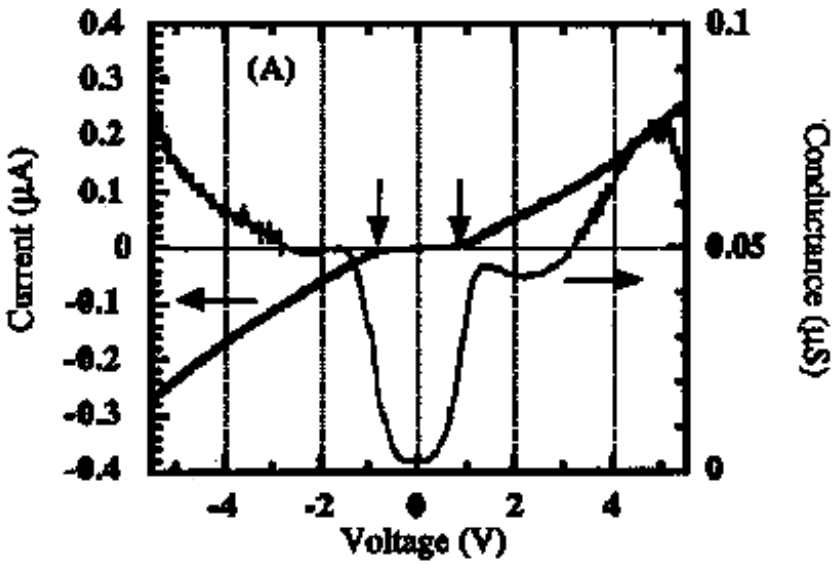

Single benzene-1,4-dithiolate molecule between atomically-sharp gold electrodes

Can this approach be applied to hydrogen storage on nanosized metal powders?

M.A. Reed, C. Zhou, C.J. Muller, T.P. Burgin, and J.M. Tour, “Conductance of a Molecular Junction”, Science, 278, 252-254 (1997).

Hydrogen Production by Grinding of Powders

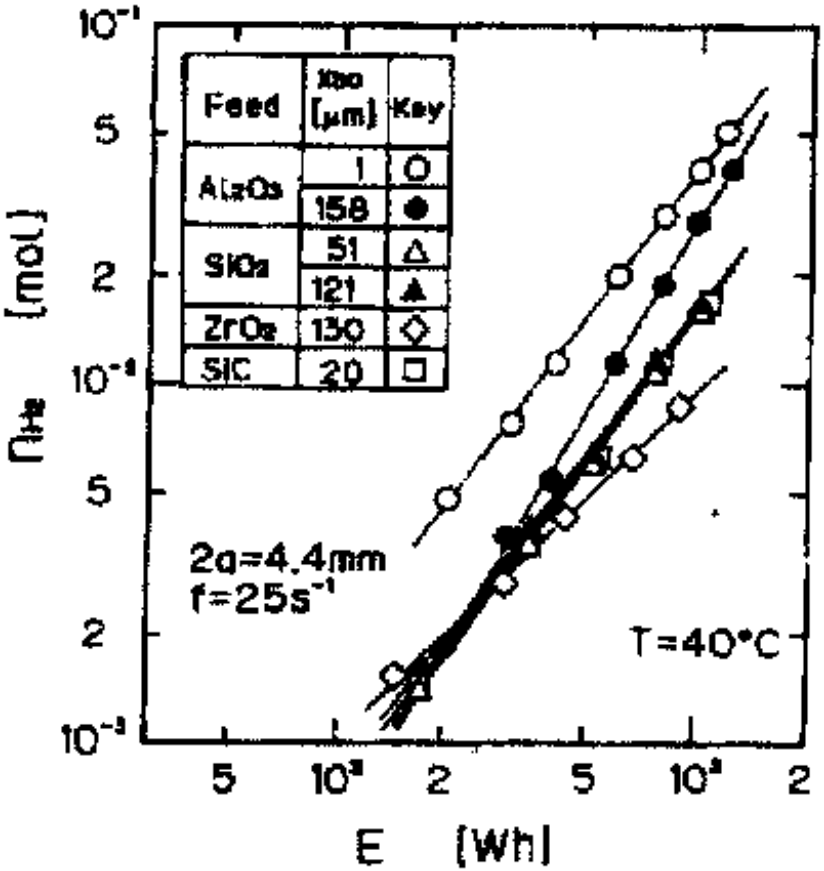

- "In wet grinding in liquid media including water or alcohol, it has been confirmed that a considerable amount of hydrogen is generated and causes an abnormal increase in pressure of a closed mill pot, even when the feed materials hardly react with them."
- Steel milling balls used to mill ceramic materials react with water to form hydrogen
- **$3\ Fe + 4\ H_2O = Fe_3O_4 + 4\ H_2$**
  - 3.3 wt.% H_2 including both Fe and H_2O

T. Yokoyama, G. Jimbo, T. Nishimura, and S. Sakai, "Effect of Fineness of Wear Particles From Steel Balls on the Rate of Hydrogen Generation During Wet Grinding of Hard Materials in Water", Powder Technology, 73, 43-49 (1992).

Hydrogen Storage in Modified Iron Oxides

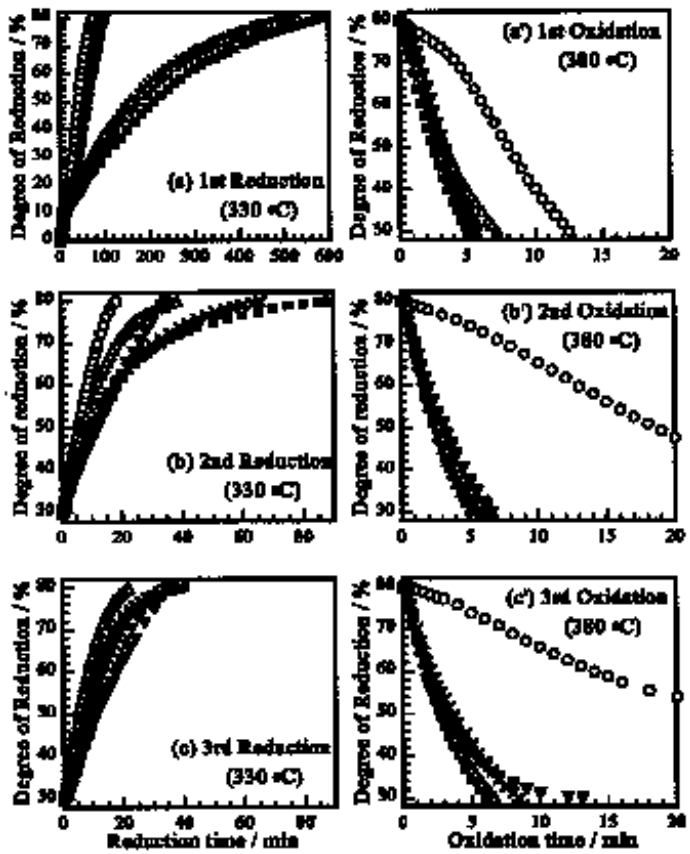

Fig. 1. Changes in the degree of reduction of Fe-oxides with and without additives as functions of reaction time for 1st to 3rd redox cycles. Additives: none (○), Ga (■), V (×), Cr (△) and Mo (▼).

H_2 Storage: $Fe_3O_4 + 4H_2 = 3Fe + 4H_2O$

H_2 Recovery: $3Fe + 4H_2O = Fe_3O_4 + 4H_2$

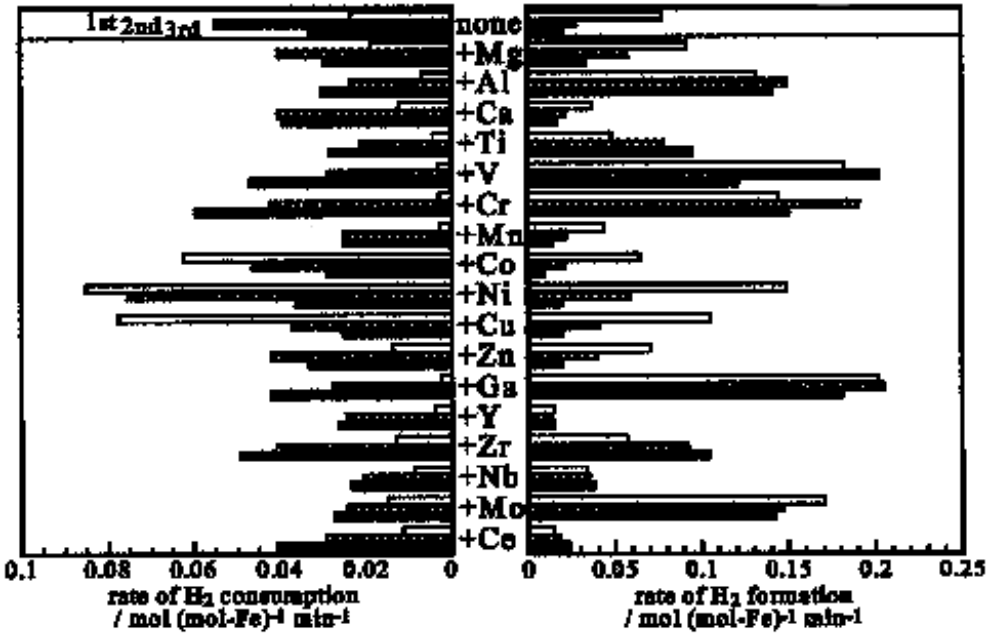

Fig. 2. Average rates of redox reactions for Fe-oxides with and without additives. Rate at 1st (□), 2nd (■) and 3rd (▨) cycles.

- **Additives accelerate reduction and oxidation reactions at lower temperatures**
  - **Al, Cr, Zr, Ga, V the most effective**

K. Otsuka, C. Yamada, T. Kaburagi, and S. Takenaka, "Storage and Generation of Pure Hydrogen by Utilization of Modified Iron Oxides", Proceedings, 14th World Hydrogen Energy Conference, June 2002, Montreal, Canada.

Hydrogen Production by the Optimized Milling of Iron Powders

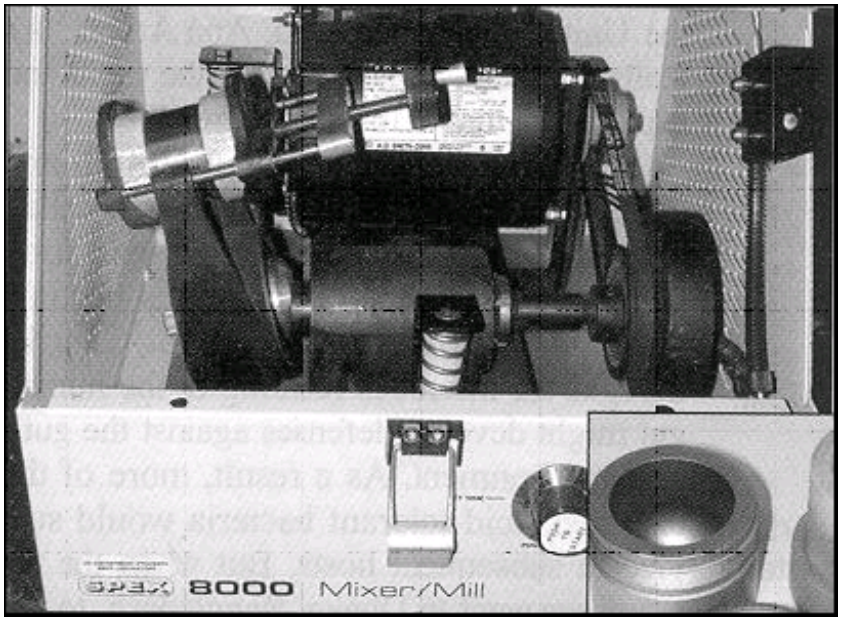

Spex shaker mill used for the mechanical alloying of materials

Concept:

- Cartridges filled with Fe powder, water, and Al_2O_3 balls (or powder)
- Mechanically vibrating the cartridge produces hydrogen gas
  - $3Fe + 4H_2O = Fe_3O_4 + 4H_2$
  - Possibility of using ultrasonic agitation
- Replace cartridge when Fe is exhausted
- Recycle spent cartridges by heating in hydrogen gas
  - $Fe_3O_4 + 4H_2 = 3Fe + 4H_2O$

Advanced Concepts Summary

- **A number of new approaches for hydrogen storage can be identified from the recent technical literature**
  - **Advanced hydride materials**
  - **Hydride "alcoholysis"**
  - **BN nanotubes**
  - **Zeolites**
  - **Mesoporous materials**
  - **Nanosize metal powders**
  - **Hydrogen from iron hydrolysis**

- **Additional study is required to establish the viability of these approaches for achieving the goal of significant improvements in hydrogen storage**